Controlled Prelithiation of PbS to Pb/Li_2S for High Initial Coulombic Efficiency in Lithium Ion Batteries

Alan Guo,[1] Eric Chen,[2] Adam Heller,[2,*] and C. Buddie Mullins [1,2,3,4,,z]**

[1]*Department of Chemistry, University of Texas at Austin, Texas 78712-1589, USA*
[2]*McKetta Department of Chemical Engineering, University of Texas at Austin, Texas 78712-1589, USA*
[3]*Texas Materials Institute, University of Texas at Austin, Texas 78712-1589, USA*
[4]*Center for Electrochemistry, University of Texas at Austin, Texas 78712-1589, USA*

PbS nanoparticle aggregates were synthesized in a simple aqueous reaction at room temperature, and were tested as a lithium ion anode material, with a gravimetric capacity of 374 mAh/g at C/2, and a 0.15% capacity loss per cycle. However, its half cell initial Coulombic efficiency (ICE) was only 40%, due to a combination of irreversible Li_2S and solid electrolyte interface (SEI) formations. A custom controlled prelithiation technique was then applied to the PbS electrodes, converting the active material to Pb/Li_2S, and consolidating the SEI prior to coin cell assembly. This brought the ICE from 40% to >97%, and allowed for immediate cycling of the electrode at high Coulombic efficiency, without further formation cycles. Upon construction of prelithiated Pb/Li_2S vs NCM full cells, an 82% ICE was observed, with the majority of the lithium loss from the NCM. The full cells had a combined electrode capacity of 100 mAh/g at C/2.

 [DOI: 10.1149/2.0641910jes]

Manuscript submitted February 22, 2019; revised manuscript received May 28, 2019. Published June 10, 2019.

Since its commercialization in the early 1990s, the lithium ion battery has used graphite as its anode material, which is limited to a theoretical capacity of 372 mAh/g, with a lithiated state of LiC_6, in a layered configuration.[1] By comparison, other Group 14 elements (M = Si, Ge, Sn, Pb) can store lithium in a $Li_{15}M_4$ alloy structure, leading to higher capacities of as much as 453 mAh/g for Pb and 3579 mAh/g for Si.[1,2] While silicon has been heavily investigated in the last two decades, lead has received little attention. Lead's heavier weight yields a lower gravimetric capacity. However, its potential for volumetric capacity (Ah/L) rivals that of silicon, at 1937 Ah/L in the lithiated state, more than double that of graphite.[1] Furthermore, lead already has a well-developed recycling infrastructure, resulting in over 99% restoration in North America, stemming from the usage of lead acid batteries in the automobile industry, thus making it environmentally benign.[3,4] Lead is therefore an attractive candidate as an anode material that warrants further investigation.

The major challenge with alloying Group 14 elements is a volume expansion of around 300% during lithiation, compared to that of graphite which is 10%.[1,5,6] This leads to excessive stress on the active material, resulting in rapid capacity loss from particle pulverization, delamination, and continuous parasitic side reactions of electrolyte decomposing onto the active material surfaces, forming a solid electrolyte interface (SEI). Over the last 10 years, various techniques have been used to help alleviate this capacity loss, such as using nanostructures to reduce particle strain, group 16 chalcogenide additives that act to buffer volume expansion, and carbon coating to passivate particle surfaces, some of which have been applied to lead based anodes.[7–14]

The usage of different group 16 chalcogenides to stabilize the cycling stability of lead has been demonstrated by Wood and coworkers.[7,10,11] Within this group (O, S, Se, Te), there is a general improvement in performance with increased atomic number, due to greater atomic radii and polarizability, leading to improved electrical and Li^+ conductivity. However, Se and Te are less abundant than S by 4 and 5 orders of magnitude, respectively, making them much more expensive, and less practical for potential commercial use. In turn, using PbS provides a good balance in terms of performance and cost as a potential battery electrode material.

While lead based anodes have been demonstrated in half cells, and full battery studies such as $LiCoO_2$/PbS have been reported,[15] the full cell studies do not include storage capacities or cycling stability. A major challenge in using PbS in a full cell is the irreversible formation of Li_2S during its first cycle to Pb/Li_2S, leading to low ICE. In this study, we eliminate this initial lithium loss by converting the unlithiated PbS electrodes to prelithiated Pb/Li_2S, before it is placed inside the coin cell. Various methods of prelithiation on silicon anodes have been demonstrated.[16–19] However, these prelithiation techniques are disadvantaged by by the following aspects:

1. The prelithiation is typically performed by direct contact of the electrode with lithium, causing a rapid lithiation that can lead to uneven SEI formation and excess stress on the electrode material.[20,21]
2. The prelithiation is typically done to completion, meaning the fully lithiated anode can only be used with unlithiated cathodes such as sulfur and vanadium oxide,[16,19,22] and excluded from common commercial lithiated cathodes like LCO, NCM and NCA.

For these reasons, the prelithiation process has to be controlled. Kim, H. et al. have demonstrated controlled partial prelithiation of silicon monoxide.[17] In this study, we further demonstrated the concept of controlled prelithiation by implementing a protocol, with improved precision, which also serves as an efficient SEI formation step, leading to improved Coulombic Efficiency (CE) in the first and subsequent cycles, and allowing the electrode to cycle at high CE in a full cell, without additional formation cycles.

Experimental

Synthesis of PbS nanoparticles.—1g of $Pb(NO_3)_2$ was dissolved in 50 mL DI water. An equimolar amount of Na_2S was dissolved in another 50 mL of DI water. Under vigorous stirring, the two solutions were quickly mixed, forming a PbS precipitate. After 10 minutes of stirring, the precipitates were centrifuged, and washed three times with 1:1 v/v DI water: ethanol, and dried overnight at 80°C under vacuum. SEM and XRD characterizations of the PbS were performed using a FEI Quanta 650 and Rigaku R-Axis Spider, respectively. Unused PbS powder was stored under argon, to prevent oxidation.

Electrode preparation.—The active material, carbon additive, and binder weight ratio was kept at 8:1:1 for all electrodes. In a 1.8 mL glass vial, 200 mg PbS was mixed with Timcal Super P, and 6 ZrO_2 pellets of 3 mm in diameter. The active material was dry milled with Super P and ZrO_2 pellets for 1 minute using a vortex mixer (Fisher Vortex Genie 2) at 10/10 intensity. 1.386 mL of water was added to the glass vial, and the slurry was vortexed at 8/10 intensity for 30 minutes. Carboxymethylcellulose (CMC, 90 kDa, Sigma Aldrich) powder was added, and the slurry was agitated with the vortex mixer at an 8/10

*Electrochemical Society Fellow.
**Electrochemical Society Member.
zE-mail: mullins@che.utexas.edu

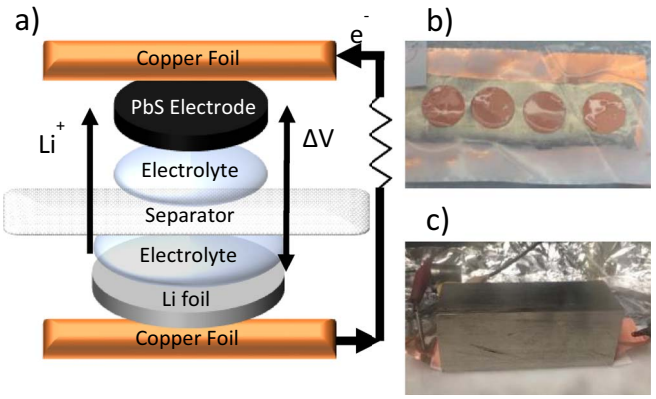

Figure 1. Schematic of prelithiation setup (a). Experimental setup of prelithiation of PbS electrodes with bottom current collector, lithium foil, wetted separator, and 4 PbS electrodes (b). Complete prelithiation setup, with top current collector, a 2 lbs weight, and alligator clips connecting to the Arbin instrument (c).

intensity for 30 minutes. Compared to one-step mixing, this multi-step addition improves slurry homogeneity, and reduces agglomeration of Super P and CMC.[23,24] The slurry (not including the ZrO_2 pellets) was then sonicated for 30s in a bath sonicator, to eliminate air bubbles, and then immediately cast onto copper foil using a doctor blade (MTI), at a 50 μm gap and 40 mm/s velocity. The electrode was then dried under vacuum at 80°C for 6 hours. The resulting electrodes were ∼4 um thick, with 1.0 mg/cm^2 of PbS mass loading.

Controlled prelithiation of PbS electrodes.—Prelithiation of PbS electrodes was performed inside an argon filled glove box prior to coin cell assembly, as illustrated in Figure 1a. Lead electrodes were stacked in parallel on top of lithium foil (99.9%, 0.75 mm thick, Alfa Aesar), separated by a separator sheet (Celgard). Each side of the separator was wetted by 1:1 v/v. fluorinated ethylene carbonate (FEC): diethyl carbonate (DEC), with 1M lithium hexafluorophosphate ($LiPF_6$). Copper foil was placed on both sides to be used as current collectors, while the separator ensured both sides were electrically insulated from each other. An ∼2 pound rectangular block was placed on top of the stacked cell, in order to ensure good contact between the layers. The two copper foils were then connected via alligator clips to an Arbin BT-2043 battery tester (Figures 1b and 1c).

The electrodes were then prelithiated using a modified formation/prelithiation cycling protocol,[25] as shown in Figure 2. Our protocol consists of 3 parts:

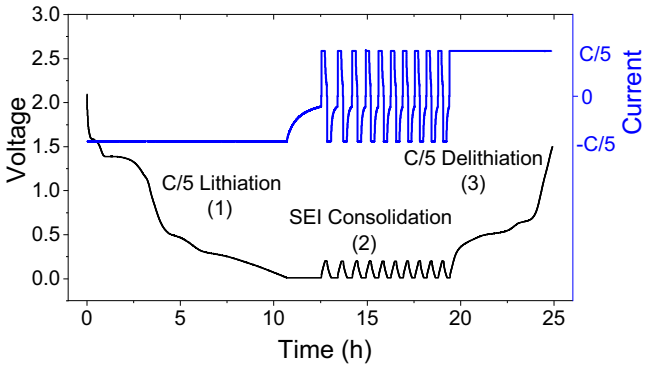

Figure 2. Prelithiation/formation cycling protocol used for PbS electrodes. Negative current refers to lithiation of the PbS electrode. 1). Full lithiation to 0.01V vs Li/Li+ 2). 0.01–0.2V cycles 3). Full delithiation to 1.5V vs Li/Li+. Each C/5 constant current cycle is followed by a constant voltage step, where voltage is maintained until magnitude of current falls below C/20.

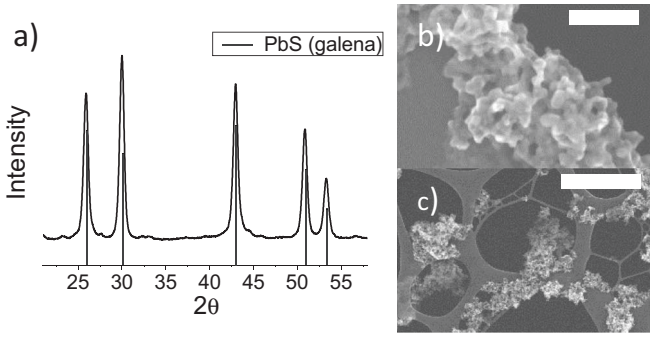

Figure 3. XRD spectrum of synthesized PbS galena (a) and SEM images of PbS nanoparticle aggregates, with scale bars of 100 nm (b) and 1000 nm (c).

1. Full lithiation of the working electrodes at C/5 to 0.01V vs Li/Li$^+$
2. 10 short SEI consolidation cycles between 0.01 and 0.2V vs Li/Li$^+$
3. Full delithiation of the working electrodes to 1.5V vs Li/Li$^+$.

At the end of each C/5 cycle, a constant voltage step was applied, long enough for the current to fall below C/20, allowing for a more complete charge/discharge cycle. Upon completion, the electrodes were immediately assembled into coin cells for electrochemical testing.

Electrochemical testing.—For half cells, 2032 coin cells were fabricated with PbS electrodes, Li foil, polypropylene separators and 1M LiPF6 1:1 v/v FEC:DEC, the same electrolyte used during prelithiation. Cyclic voltammetry scans of half cells were performed at 0.1 mV/s between 0.01–1.5V vs Li/Li$^+$. PbS half cells were constructed, underwent the same prelithiation/formation protocol described earlier, and were cycled 10 times at various C-rates in the following order: C/5, C/2, 1C, 2C, 5C, 1C and C/2. Additional PbS half cells, prepared in the same manner, were cycled at C/2 for 100 cycles. For full cells, PbS electrodes were first prelithiated using the procedure described in the previous section, and were then assembled into coin cells with $Li(NiCoMn)_{1/3}O_2$ (NCM 111), using a 1.05–1.1 N/P (negative/positive) electrode capacity ratio. For comparison, unlithiated PbS electrodes were assembled with NCM into full cells, in the same manner, using a standard C/20 formation cycle. All full cells were then cycled between 2.7–4.2V at C/2 for 100 cycles. Sulfur dissolution is avoided, as the typical voltage range for the Li_2S electrode is 1.7–2.5V.

Results and Discussion

Material characterization.—Figure 3a shows XRD measurements of the PbS material, indicating the *galena* crystal structure. SEM images of the PbS material show polydisperse nanoparticle aggregates (Figures 3b and 3c). Aggregation likely occurred as a result of the highly spontaneous reaction between Pb^{2+} and S^{2-} upon mixing.

Effects of prelithiation on initial coulombic efficiency.—Initial charge/discharge cycles and cyclic voltammetry of unlithiated PbS and prelithiated Pb/Li_2S half cells are shown in Figure 4. Upon initial lithiation of the PbS (unlithiated) electrode, sulfur was irreversibly reduced (Figure 4c), leading to a loss of 31–36% in ICE, estimated from the formation of Li_2S and a fully lithiated state of Li_xPb, where $3.5 < x < 4.5$.[26] The first lithiation cycle was also characterized by a large baseline current, attributed to SEI formation, resulting in an overall ICE of only 40% (Figure 4a). By contrast, the prelithiated Pb/Li_2S electrode shows only 3% lithium loss in the first cycle (Figures 4b, 4d). Electrode thicknesses (without current collector) before and after prelithiation were measured with digital calipers to be around 4 and 10 μm, respectively.

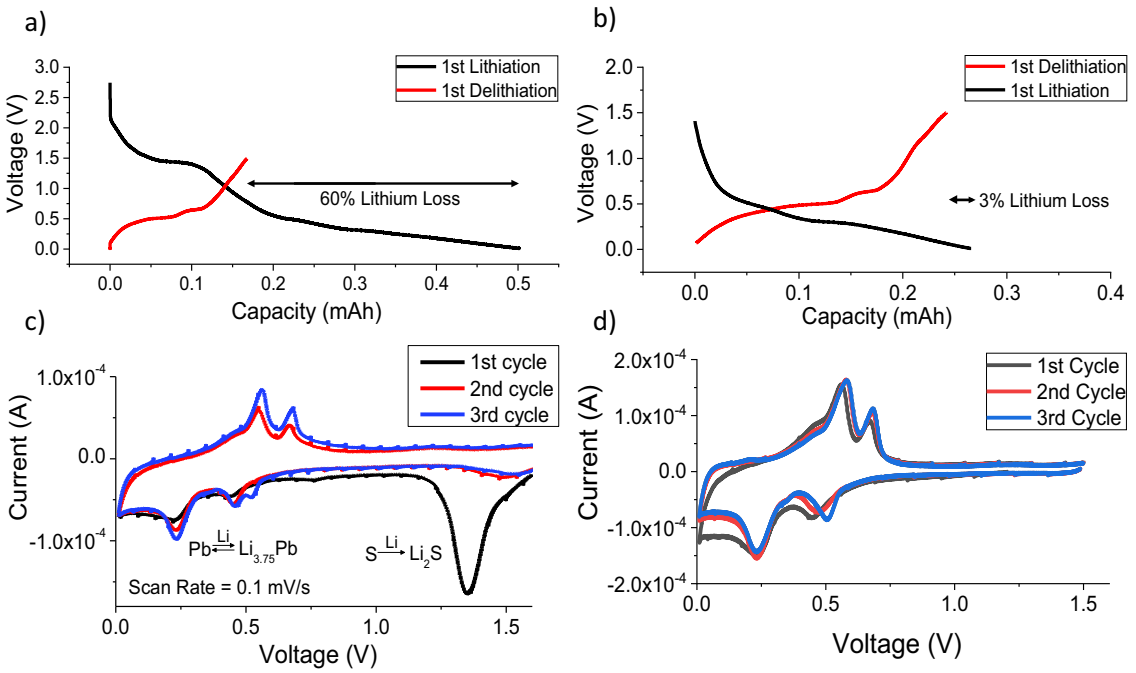

Figure 4. First charge/discharge cycle of unlithiated PbS half cell (a), First charge/discharge cycle of prelithiated PbS half cell (b), Cyclicvoltammetry of unlithiated half cell (c), and cyclic voltammetry of prelithiated half cell (d).

The reason for the 0.01–0.2V cycles during prelithiation/formation was that at near full lithiation, there was a greater abundance of lithium that could react with the electrolyte. As a result, the majority of the SEI would form on the electrode in the lithiated state.[27–29] Figure 5a shows the CE for each 0.01–0.2V cycle was drastically lower than what is expected from a full 0.01–1.5V cycle. This confirms that a greater percentage of lithium reacted to form the SEI, allowing for more efficient formation cycles, leading to faster SEI consolidation. Furthermore, the CE of each consecutive 0.01–0.2V cycle is drastically greater than the cycle preceding it, indicating less Li was lost to SEI formation, and a more complete SEI layer. Depending on the material, the number of 0.01–0.2V cycles can be easily customized, with relatively little impact on completion time.

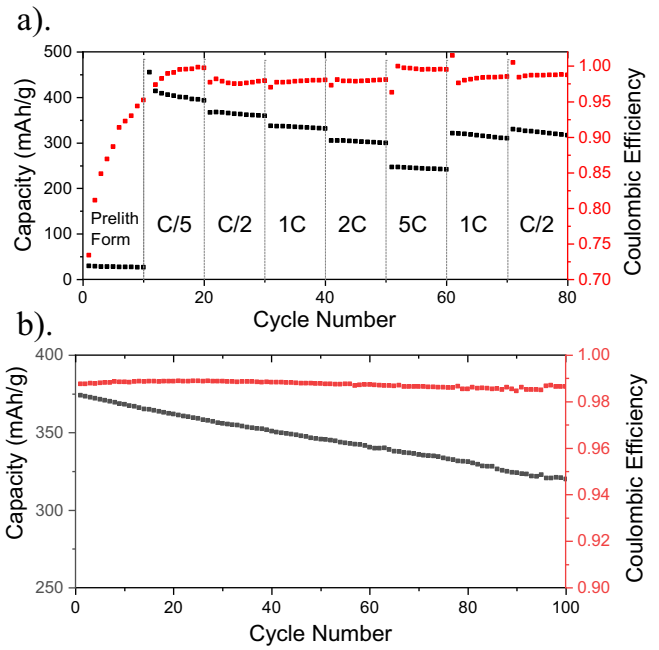

Figure 5. Half cell performance of prelithiated PbS electrodes at various C-rates (a), where cycles 1–10 show SEI consolidation cycles 0.01–0.20 vs Li/Li+. The C-rate was then varied at C/5, C/2, 1C, 2C, 5C, 1C and C/2. PbS electrodes were also cycled for 100 cycles at C/2 (b), averaging 0.15% capacity fade per cycle.

Half cell performance.—Reversible capacities for the PbS electrodes at C/5, C/2, 1C, 2C, and 5C were 410, 367, 337, 305, and 247 mAh/g, respectively (Figure 5a). C-rate currents were based on the theoretical capacity of 420 mAh/g for PbS. Upon extended cycling at C/2 (Figure 5b), the electrodes experienced 0.15% capacity loss/cycle. The relatively stable cycling of the PbS, compared to other lead based active materials, is attributed to the stabilization of Li_2S, and the semi-porous nature of the nanoparticle aggregates (Figures 3b–3c), which helped accommodate volume expansion.[30–34] The initial Coulombic Efficiencies (ICE) of the prelithiated Pb/Li_2S half cells were 97.5% and 98.8% for C/5 and C/2, respectively (Figure 5).

Full cell performance.—Prelithiated Pb/Li_2S electrodes were put inside full cells with NCM (111) cathode electrodes, and cycled at C/2. The capacity ratio between the negative and positive electrodes (N:P ratio) was kept between 1.05–1.1 for all full cells, in order to prevent Li plating on the anode. Figure 6a shows full cell performances of prelithiated Pb/Li_2S electrodes, compared to the performance of unlithiated PbS electrodes. Initial electrode capacities at C/2 were 374 mAh/g for Pb/Li_2S (Figure 6), and 140 mAh/g for NCM (Figure S-2), resulting in a combined full cell capacity of 102 mAh/g (Figure 6a). The ICE of the prelithiated full cells cycled at C/2 was 82.0% (Figure 6b). The majority of this lithium loss is attributed to the NCM cathode, which generally has an 85% ICE (Figure S-2).[35] By contrast, the ICE of the unlithiated PbS full cells, which used a standard C/20 formation cycle, was only 20% (Figures 6b and 6d), even lower than the 40% observed in unlithiated PbS half cells. This is because the redox potential of sulfur is much higher than that of lead (Figure 4c), such that the first charge cycle was more selective towards lithiating sulfur instead of lead. A much larger cathode would be required in order to fully lithiate the unlithiated PbS electrode. Following the first cycle, the CE of the prelithiated Pb/Li_2S electrodes normalized to

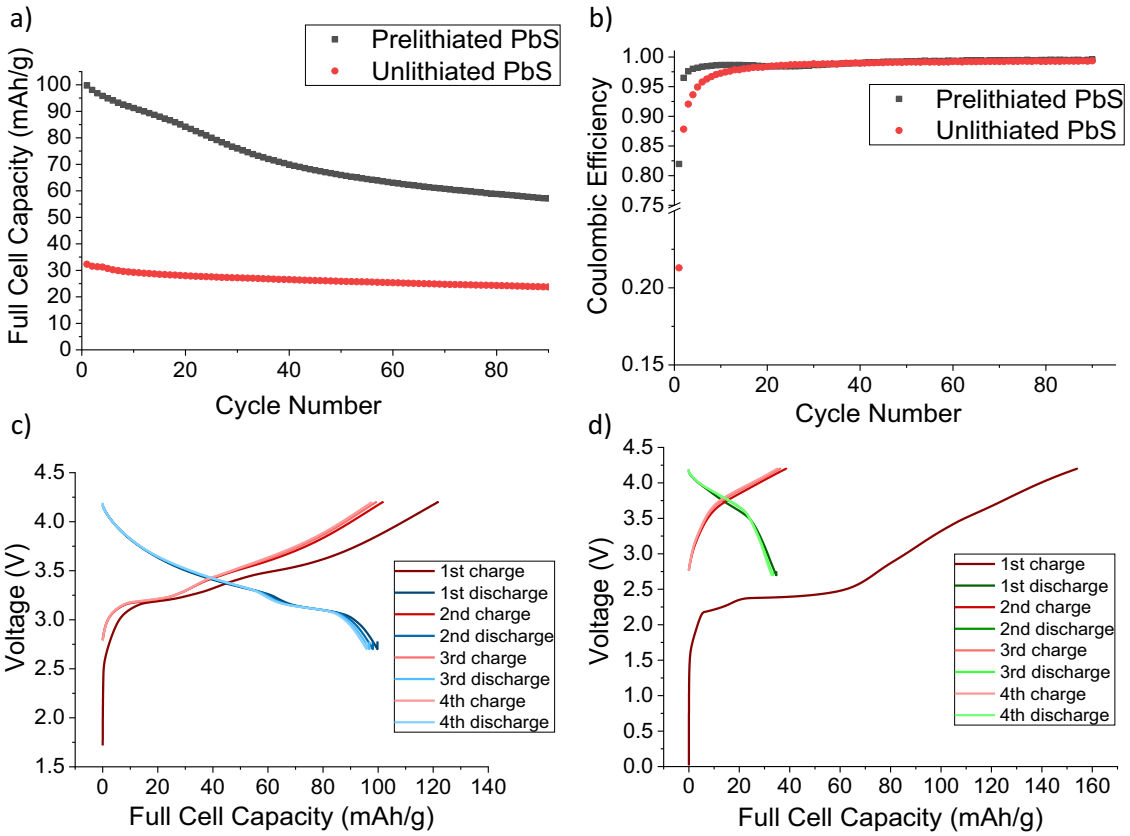

Figure 6. Active material capacities of prelithiated PbS-NCM full cells and non-prelithiated PbS-NCM full cells at C/2 (a), and their respective Coulombic Efficiencies (b). Charge/discharge curves of full cells with prelithiated PbS electrodes (c), and charge/discharge curves of full cells with non-prelithiated PbS electrodes (d).

98–99% within 2 cycles, while the CE of the unlithiated PbS electrodes reached 98% after 20 cycles (Figure 6b). This shows that the advantages of our prelithiation protocol extend beyond just the first cycle, largely due to the 0.01–0.2V SEI consolidation cycles, as illustrated by the CE in the prelithiation cycles (Figure 5a). Despite this, the unlithiated PbS electrodes showed more stable cycling. This was because the effective state of charge (SOC) of these electrodes were much lower than those of the prelithiated PbS electrodes, due to the lower ICE, leading to less volume expansion, and stress on the electrodes. The greater capacity fade of the prelithiated Pb/Li_2S full cells (Figure 6a) relative to their half cell counterparts (Figure 5b) reflects the limited source of lithium in the full cells, combined with the long term CE of the anode (98–99%). During extended cycling, the active material expands and contracts, exposing new surfaces to the electrolyte, forming additional SEI, leading to further lithium loss, indicated by the lower CE. Surface treatment such as carbon coating has been

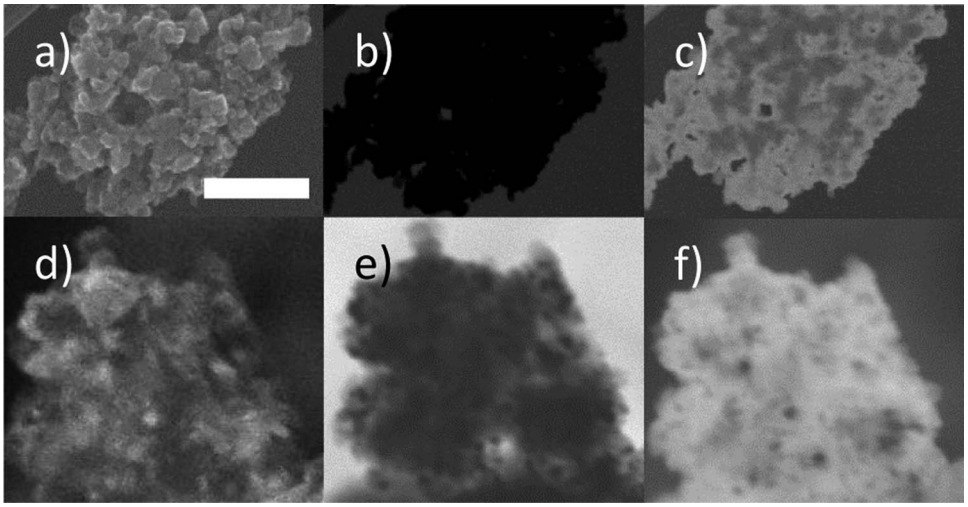

Figure 7. SEM, BF and DF STEM (a-c, respectively) scans of PbS nanoparticle aggregate before cycling. SEM, BF and DF STEM (d-f, respectively) scans of PbS electrode material after 200 cycles. Scale bar represents 200 nm for all images.

demonstrated help mitigate this issue in lead based anodes, improving the CE.[36]

Post-mortem analysis.—After 200 cycles, Pb/Li_2S half cells were completely delithiated to 1.5V vs Li/Li^+ and disassembled. Bright Field (BF) and Dark Field (DF) STEM scans of the cycled electrode (Figures 7b, 7c) show much greater electron penetration, compared to that of uncycled PbS (Figures 7b, 7c). This indicates a lower material density and higher porosity in the cycled PbS, which is consistent with volume expansion from Pb lithiation.

Conclusions

For the first time, full cells were created with a lead based anode, using PbS. The cells were tested employing two different types of lead sulfide anodes: (i) a lead sulfide anode that was prelithiated to create a composite active material Pb/Li_2S and (ii) a PbS active material that was not prelithiated. The controlled prelithiation protocol used not only improved the half cell ICE from 40% to >97% (compared to the unlithiated anode), but also helped form a more complete SEI layer, which allowed the electrodes to perform at high CE, without additional formation cycles. The prelithiated Pb/Li_2S electrodes showed a 374 mAh/g half cell capacity at C/2, and a combined electrode capacity of 102 mAh/g capacity when cycled with an NCM cathode.

Acknowledgments

We acknowledge the generous support provided by the Welch Foundation (via Grants F-1131 (A.H.) and F-1436 (C.B.M.)) as well as the National Science Foundation via Grant CBET-1603491. We also thank Celgard Corp. for their provision of separators, and Solvay Fluor for their donation of the fluoroethylene carbonate.

ORCID

C. Buddie Mullins https://orcid.org/0000-0003-1030-4801

References

1. M. N. Obrovac and V. L. Chevrier, Alloy negative electrodes for Li-ion batteries. *Chem. Rev.*, **114**, 11444 (2014).
2. Huajun Tian, Fenxia Xin, Xiaoliang Wang, and Wei He, W. H. High capacity group-IV elements (Si, Ge, Sn) based anodes for lithium-ion batteries. *J. Mater.*, **1**, 153 (2015).
3. R. Jolly and C. Rhin, The recycling of lead-acid batteries: production of lead and polypropylene. *Resour. Conserv. Recycl.*, **10**, 137 (1994).
4. A. Darwiche, R. Dugas, B. Fraisse, and L. Monconduit, Reinstating lead for high-loaded efficient negative electrode for rechargeable sodium-ion battery. *J. Power Sources*, **304**, 1 (2016).
5. J. W. Choi and D. Aurbach, Promise and reality of post-lithium-ion batteries with high energy densities. *Nat. Rev. Mater.*,**1**, (2016).
6. Y. Qi, L. G. Hector, C. James, and K. J. Kim, Lithium Concentration Dependent Elastic Properties of Battery Electrode Materials from First Principles Calculations. *J. Electrochem. Soc.*, **161**, F3010 (2014).
7. S. M. Wood, E. J. Powell, A. Heller, and C. B. Mullins, Lithiation and Delithiation of Lead Sulfide (PbS). *J. Electrochem. Soc.*, **162**, A1182 (2015).
8. C.-H. Li, P. Sengodu, D.-Y. Wang, T.-R. Kuo, and C.-C. Chen, Highly stable cycling of a lead oxide/copper nanocomposite as an anode material in lithium ion batteries. *RSC Adv.* **5**, 50245 (2015).
9. M. Martos, J. Morales, and L. Sánchez, Lead-based systems as suitable anode materials for Li-ion batteries. *Electrochim. Acta*, **48**, 615 (2003).
10. S. M. Wood, C. H. Pham, A. Heller, and C. B. Mullins, Formation of an Electroactive Polymer Gel Film upon Lithiation and Delithiation of PbSe. *J. Electrochem. Soc.*, **163**, A1666 (2016).
11. S. M. Wood, K. C. Klavetter, A. Heller, and C. B. Mullins, Fast lithium transport in PbTe for lithium-ion battery anodes. *J. Mater. Chem. A*, **2**, 7238 (2014).
12. Q. Pan, Z. Wang, J. Liu, G. Yin, and M. Gu, PbO@C core-shell nanocomposites as an anode material of lithium-ion batteries. *Electrochem. commun.*, **11**, 917 (2009).
13. M Martos et al. Electrochemical properties of lead oxide films obtained by spray pyrolysis as negative electrodes for lithium secondary batteries. *Electrochim. Acta*, **46**, 2939 (2001).
14. Z. Yuan, Z. Peng, Y. Chen, and H. Liu, Synthesis and electrochemical performance of nanosized tin lead composite oxides as lithium storage materials. *Mater. Chem. Phys.*, **120**, 331 (2010).
15. A. Sanusi, M. Z. A. Yahya, S. Navaratnam, W. J. Basirun, Y. Alias, and N. S. Mohamed, A. K. A. Sulphide based anode material for lithium rechargeable battery. *Ionics (Kiel)*. 253 (2003).
16. F. Holtstiege, P. Bärmann, R. Nölle, M. Winter, and T. Placke, Pre-Lithiation Strategies for Rechargeable Energy Storage Technologies: Concepts, Promises and Challenges. *Batteries*, **4**, 4 (2018).
17. H. J Kim et al. Controlled Prelithiation of Silicon Monoxide for High Performance Lithium-Ion Rechargeable Full Cells. *Nano Lett*. **16**, 282 (2016).
18. I. C. Stefan and Y. Cohen, A Commercially Scalable Process for Silicon Anode Prelithiation. (2015).
19. N. Liu, L. Hu, M. T. Mcdowell, A. Jackson, and Y. Cui, Prelithiated Silicon Nanowires as an Anode for Lithium Ion Batteries. *ACS Nano*, 6487 (2011).
20. S. J. An et al. The state of understanding of the lithium-ion-battery graphite solid electrolyte interphase (SEI) and its relationship to formation cycling. *Carbon N. Y.*, **105**, 52 (2016).
21. S. S. Zhang, A review on electrolyte additives for lithium-ion batteries. *Journal of Power Sources*, (2006).
22. J. Zhao et al. Air-stable and freestanding lithium alloy/graphene foil as an alternative to lithium metal anodes. *Nat. Nanotechnol.*, 1 (2017).
23. V. Wenzel, H. Nirschl, and D. Nötzel, Challenges in Lithium-Ion-Battery Slurry Preparation and Potential of Modifying Electrode Structures by Different Mixing Processes. *Energy Technol*. **3**, 692 (2015).
24. A. Kraytsberg and Y. Ein-Eli, Conveying Advanced Li-ion Battery Materials into Practice The Impact of Electrode Slurry Preparation Skills. *Adv. Energy Mater.*,**6**, (2016).
25. S. J. An, J. Li, Z. Du, C. Daniel, and D. L. Wood, Fast formation cycling for lithium ion batteries. *J. Power Sources*, **342**, 846 (2017).
26. S. M. Wood, C. H. Pham, A. Heller, and C. B. Mullins, Communication — Stages in the Dynamic Electrochemical Lithiation of Lead. *J. Electrochem. Soc.*, **163**, A1027 (2016).
27. P. Lu, C. Li, E. W. Schneider, and S. J. Harris, Chemistry, impedance, and morphology evolution in solid electrolyte interphase films during formation in lithium ion batteries. *J. Phys. Chem. C*, **118**, 896 (2014).
28. A. J. Smith, J. C. Burns, S. Trussler, and J. R. Dahn, Precision Measurements of the Coulombic Efficiency of Lithium-Ion Batteries and of Electrode Materials for Lithium-Ion Batteries. *J. Electrochem. Soc.*, **157**, A196 (2010).
29. S. P. Kim, A. C. T. V. Duin, and V. B. Shenoy, Effect of electrolytes on the structure and evolution of the solid electrolyte interphase (SEI) in Li-ion batteries: A molecular dynamics study. *J. Power Sources*, **196**, 8590 (2011).
30. Y. Li, H. Q. Xie, and J. P. Tu, SnS with various morphologies and sizes as anode material for lithium ion batteries. *Wuli Huaxue Xuebao/ Acta Phys. - Chim. Sin.*, **25**, 365 (2009).
31. K. C. Klavetter, J. Pedro De Souza, A. Heller, and C. B. Mullins, High tap density microparticles of selenium-doped germanium as a high efficiency, stable cycling lithium-ion battery anode material. *J. Mater. Chem. A*, **3**, 5829 (2015).
32. P. R. Abel, K. C. Klavetter, K. Jarvis, A. Heller, and C. B. Mullins, Sub-stoichiometric germanium sulfide thin-films as a high-rate lithium storage material. *J. Mater. Chem. A*, **2**, 19011 (2014).
33. P. R. Abel, Y. M. Lin, H. Celio, A. Heller, and C. B. Mullins, Improving the stability of nanostructured silicon thin film lithium-ion battery anodes through their controlled oxidation. *ACS Nano*, **6**, 2506 (2012).
34. P. R. Abel, K. C. Klavetter, A. Heller, and C. B. Mullins, Thin Nanocolumnar Ge 0.9 Se 0.1 Films Are Rapidly Lithiated/Delithiated. *J. Phys. Chem. C*, **118**, 17407 (2014).
35. X. L. Wang et al. Amorphous hierarchical porous GeO x as high-capacity anodes for Li ion batteries with very long cycling life. *J. Am. Chem. Soc.*, **133**, 20692 (2011).
36. A. Guo, E. Chen, B. R. Wygant, A. Heller, and C. B. Mullins, "Lead Oxide Microparticles Coated by Ethylenediamine-Crosslinked Graphene Oxide for Lithium Ion Battery Anodes," *ACS Appl. Energy Mater.*, **2**(5), 3017 (2019).